Environ Geol (2006) 51: 91–102
DOI 10.1007/s00254-006-0307-0

ORIGINAL ARTICLE

Chunxiang Wang
Tetsuro Esaki
Mowen Xie
Cheng Qiu

Landslide and debris-flow hazard analysis and prediction using GIS in Minamata–Hougawachi area, Japan

Received: 2 December 2005
Accepted: 18 April 2006
Published online: 13 May 2006

C. Wang (✉) · T. Esaki · C. Qiu
Institute of Environment Systems, Kyushu University, Hakouzaki 6-10-1, Higashi Ku, Fukuoka 812-8581, Japan
E-mail: wang@ies.kyushu-u.ac.jp
Tel.: +81-92-6423494
Fax: +81-92-6423848

M. Xie
College of Civil and Environment Engineering, University of Science and Technology, Beijing, Xueyuan Lu 30, Haidian District, Beijing 10083, China

Abstract On July 20, 2003, following a short duration of heavy rainfall, a debris-flow disaster occurred in the Minamata–Hougawachi area, Kumamoto Prefecture, Japan. This disaster was triggered by a landslide. In order to assess the landslide and debris-flow hazard potential of this mountainous region, the study of historic landslides is critical. The objective of the study is to couple 3D slope-stability analysis models and 2D numerical simulation of debris flow within a geographical information systems in order to identity the potential landslide-hazard area. Based on field observations, the failure mechanism of the past landslide is analyzed and the mechanical parameters for 3D slope-stability analysis are calculated from the historic landslide. Then, to locate potential new landslides, the studied area is divided into slope units. Based on 3D slope-stability analysis models and on Monte Carlo simulation, the spots of potential landslides are identified. Finally, we propose a depth-averaged 2D numerical model, in which the debris and water mixture is assumed to be a uniform continuous, incompressible, unsteady Newtonian fluid. The method accurately models the historic debris flow. According to the 2D numerical simulation, the results of the debris-flow model, including the potentially inundated areas, are analyzed, and potentially affected houses, river and road are mapped.

Keywords Landslide · Debris flow · Geographical information systems · Numerical simulation · Hazard

Introduction

Landslides and debris flows are a source of severe natural disasters and societal hazard in mountainous regions throughout the world (Guariguata 1990; Bergin et al. 1995; Walker et al. 1996; Iida 1999; Zhou et al. 2003). It has been generally recognized that the occurring of a landslide is mainly related to bedrock geology, lithology, geotechnical properties, rainfall, groundwater conditions and land-use conditions (Anbalagan 1992; Aleotti and Chowdhury 1999; Lan et al. 2004). Analyzing the relationship between landslides and the various factors causing landslides not only provides an insight to understand landslide mechanisms, but also can form a basis for predicting future landslides and assessing the landslide hazard. In areas with the similar geotechnical conditions, researchers generally make two fundamental assumptions. On the one hand, landslides will occur in the same geological, geomorphological, hydrogeological and climatic conditions as in the past. On the other hand, the properties and types of landslides will also be the same (Hutchinson 1995; Aleotti and Chowdhury 1999). Therefore, the study of the mechanisms and properties of past landslide is a valuable reference for assessing the future landslide hazard in its adjacent or geotechnically similar area.

Most debris flows originally occur in the form of rainfall-induced landslides before they move into a

valley channel (Fleming et al. 1989; Lan et al. 2004; Wen and Aydin 2005). Slides that mobilize into flows usually are characterized by high-velocity movement and long run-out distance and may present the greatest risk to human life. How to mitigate the disaster caused by landslides that mobilize into debris flows is an urgent problem. Strategies should be devised to help understand landslide processes, analyze the threatening landslide hazard and predict future landslides in order to reduce the ongoing and future damage from landslides. Therefore, prediction of the inundated area, including the potentially affected inhabited areas, is of great importance in debris-flow risk assessment.

Geographical information systems (GIS) have become a powerful tool for effective analysis and prediction associated with the study of geological hazards. This is not only because GIS has excellent data structures and spatial data-processing abilities, but also because the collection, manipulation and analysis of the environmental data on landslide and debris-flow hazard can be accomplished much more efficiently and cost effectively (Carrara and Guzzetti 1999; Guzzetti et al. 1999).

On July 19–20, 2003, a short duration high-intensity rainfall event impacted the city of Minamata in Kumamoto Prefecture, Japan (Fig. 1). This rainfall triggered many landslides and debris flows (Nakazawa et al. 2003; Iwao 2003; Taniguchi 2003). The slope failure and resultant debris flow at Hougawachi in Minamata was the largest and most damaging of these disasters (Fig. 2). A moderate-sized, 4–9-m deep debris avalanche triggered the debris flow about 1.5 km upslope of where the casualties occurred. The volume of sediment discharge plunging into the village of Minamata–Hougawachi, was estimated about 1,000,000 m^3, and the velocity of debris flow was estimated from about 2.9 to 23.5 m/s (Taniguchi 2003). The disaster killed 15 people and more than 14 houses were either damaged or destroyed. In an attempt to forecast a similar landslide-related disaster in the future, this study will concentrate on landslide hazards around the site of the July 19–20 Minamata–Hougawachi landslide. Figure 1 shows the 2.5 km by 3 km study area, the local drainage system and the location of main roads and homes.

The problem of coupling spatially distributed susceptibility or hazard assessments and numerical simulations of individual landslides is important, particularly in view of the recent developments in GIS and numerical methods. This paper aims to produce a landslide- and debris-flow hazard map in the Minamata–Hougawachi region, Kumamoto Prefecture, Japan. A two-step procedure to define landslide and debris-flow susceptibility in the study area has been attempted. First, a GIS-based 3D limit-equilibrium stability analysis model (Xie et al. 2003) is used to define the location of potential landslides. Then, according to the results of the 2D numerical simulation of debris flow, the area of potential inundation is defined, including the affected homes, river and road sections.

Analysis of the historic landslide

The slope failure occurred at 4:20 am on July 20, 2003, 4.3 h after the beginning of the rainstorm and during the period of highest rainstorm intensity (Fig. 3). The soil stratigraphy at the landslide site is schematically illustrated in Fig. 4. The landslide mass can be considered to have been triggered by a rapid increase in the pore-water pressure. The landslide mechanism was controlled by local lithological conditions, where an almost impermeable layer (map unit An-5: tuff breccia, brecciated lava and lava) is overlaid by highly weathered rock (map unit An-7, mainly lava with subordinate tuff breccia) (Fig. 5). During the intense

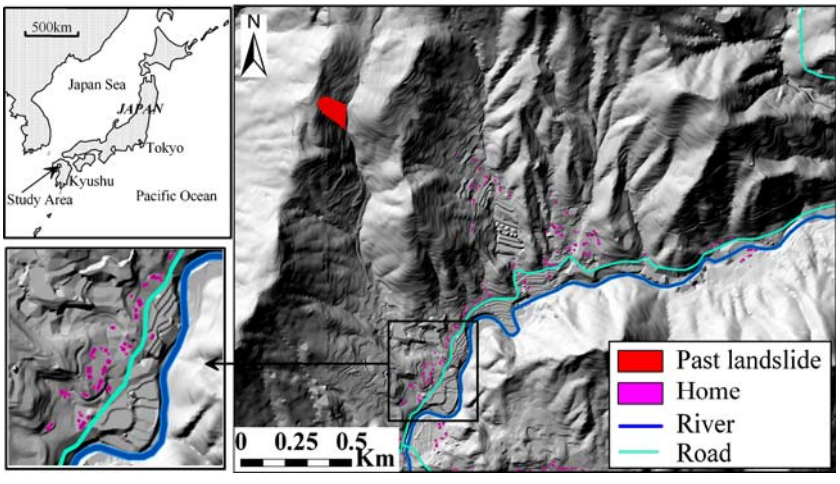

Fig. 1 Study area with distribution of homes, river and main road

Fig. 2 Aerial photograph of the debris flow at Hougawachi, Minamata city

rainfall, high pore-water pressure likely developed at the base of the weathered An-7 within the limited space in the fractures and interstices. Field surveys have indicated that almost no subsurface water infiltrated the exposed bedrock 1 week after the landslide, demonstrating the rapid accretion of pore pressure in the weathered regolith during the rainstorm. The landslide mass developed into debris flow after it entered the stream channel and impacted the village after traveling about 1.5 km in 3 min (Fig. 2).

Landslide-susceptibility map

Basic data

The study area is limited to the region containing map units An-7 and An-5 (Fig. 5). Based on a topographic map with a scale of 1:2,500, a contour-line file was generated, with a contour interval of 2 m. This file was converted to a triangulated irregular network (TIN) and subsequently a digital elevation model (DEM). The roads and streams that located in the study area were stored as polylines, and the houses as polygons.

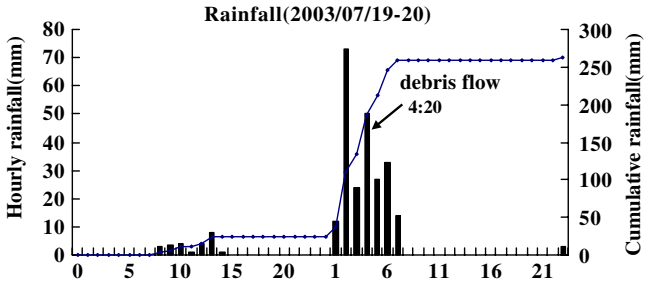

Fig. 3 Precipitation at Minamata City (July 19 0:00 to July 20 22:00, 2003)

Slope units

For the landslide-hazard assessment of a large mountainous area with complex geometry and geological conditions, a key problem is how to extract the appropriate slope unit for potential sliding-surface identification and minimum 3D safety-factor calculation. Slope unit, namely, the portion of the land surface delimited by watershed divides and channels has similar topographic and geological characteristics. The suitability of the slope units for landslide-hazard assessment and for other land-rated study has been recognized by several authors (Hansen 1984; Carrara et al. 1991; Dymond et al. 1995).

A GIS-based hydrological analysis and modeling tool, Arc Hydro (David 2002), is employed to draw watershed divides and to delineate slope units auto-

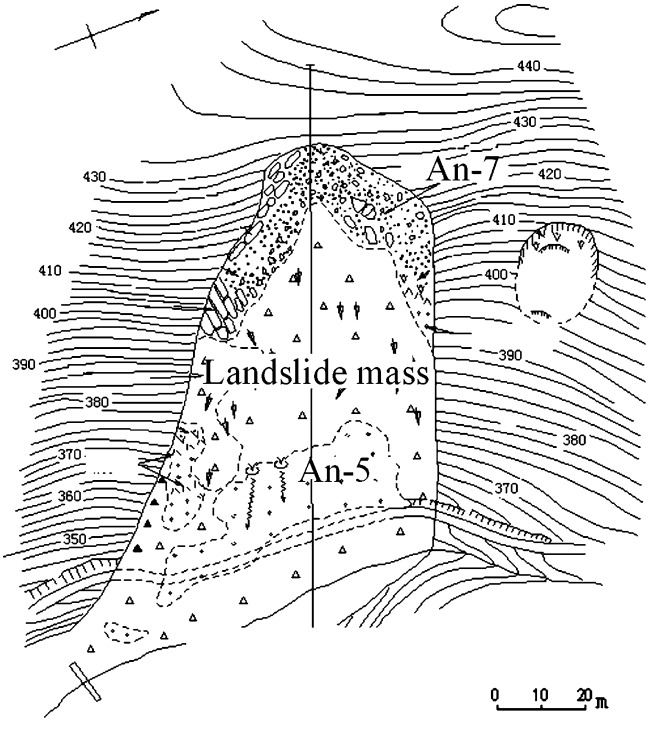

Fig. 4 Schematics of the landslide mass

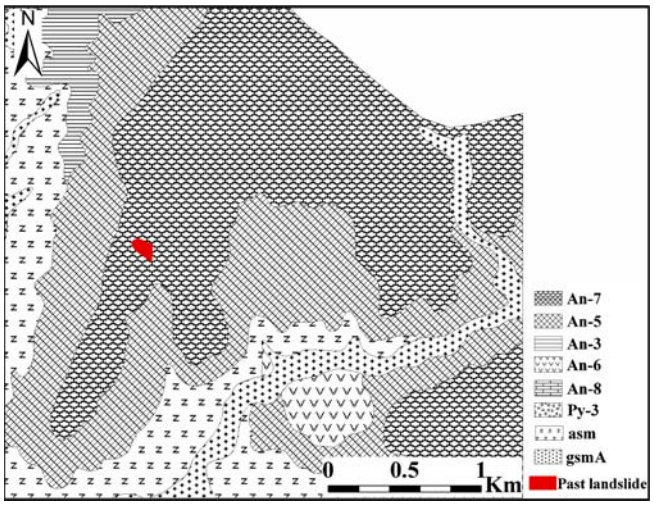

Fig. 5 Lithological map of the study area [An-3 andesitic rock-3 (tuff breccia, brecciated lava and lava), *An-5* andesitic rock-5 (tuff breccia, brecciated lava and lava), *An-6* andesitic rock-6 (neck), *An-7* andesitic rock-7 (mainly lava with subordinate tuff breccia), *An-8* andesitic rock-8 (lava), *Py-3* pyroclastics-3, *Asm* alternating beds of sandstone and mudstone; *gsmA* gravel, sand and mud (low-land sediments)]

matically from a DEM (Fig. 6) over this geologically similar study area.

Analysis of mechanical parameters

Based on the field landslide survey of July 20, 2003, the geometry of the landslide was described (Fig. 4). The engineering geological report of this area provided several pairs of mechanical parameters (Table 1). In order to determine one pair to represent the shear parameters of the sliding surface, using the geometry information in Fig. 4 and the GIS-based 3D limit-equilibrium models (Revised Hovland model, 3D extension of Bishop model and 3D extension of Janbu model) (Xie et al. 2003; Xie and Esaki 2005), the 3D safety factor with different pairs of shear parameters is calculated (Table 1).

Revised Hovland model is

$$\mathrm{SF}_{3\mathrm{D}} = \frac{\sum_j \sum_i \left(cA + (W+P)\cos\theta\tan\phi\right)\cos\theta_{\mathrm{Avr}}}{\sum_j \sum_i (W+P)\cos\theta_{\mathrm{Avr}}\sin\theta_{\mathrm{Avr}}} \quad (1)$$

3D extension of Bishop model is

$$\mathrm{SF}_{3\mathrm{D}} = \left(\sum_j \sum_i (W+P)\sin\theta_{\mathrm{Avr}}\right)^{-1} \times \sum_j \sum_i \frac{(W+P)\tan\phi + cA\cos\theta}{\cos\theta + \mathrm{SF}_{3\mathrm{D}}^{-1}\tan\phi\sin\theta_{\mathrm{Avr}}} \quad (2)$$

and 3D extension of Janbu model is

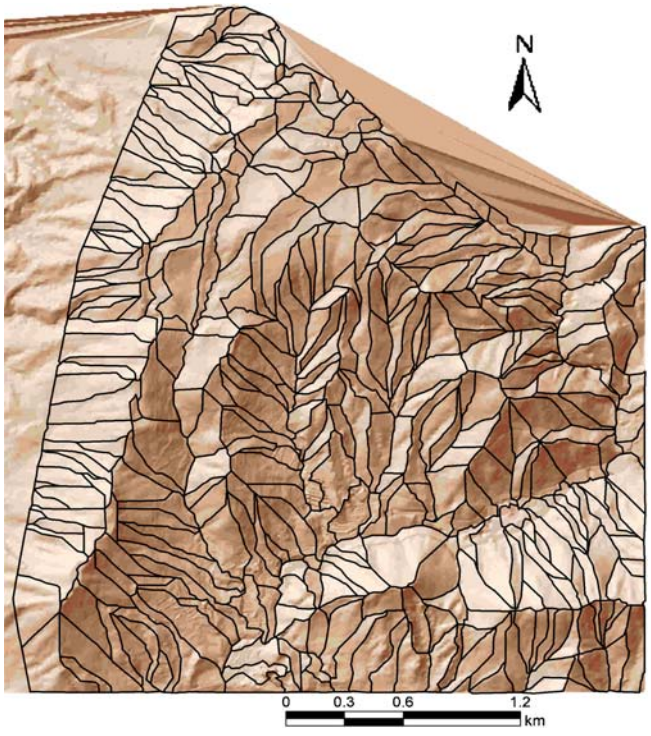

Fig. 6 Distribution of slope units

$$\mathrm{SF}_{3\mathrm{D}} = \frac{\sum_{\mathrm{j}} \sum_{\mathrm{i}} [\mathrm{cA} + \mathrm{N}\tan\phi]\cos\theta_{\mathrm{Avr}}}{\sum_{\mathrm{j}} \sum_{\mathrm{i}} \mathrm{N}\sin\theta\cos\left(\theta_{\mathrm{Asp}} - \theta_{\mathrm{AvrAsp}}\right)}, \quad \mathrm{N} = \frac{\mathrm{P} + \mathrm{W} - \mathrm{SF}_{3\mathrm{D}}^{-1}\mathrm{cA}\sin\theta_{\mathrm{Avr}}}{\cos\theta + \mathrm{SF}_{3\mathrm{D}}^{-1}\tan\phi\sin\theta_{\mathrm{Avr}}} \quad (3)$$

where $\mathrm{SF}_{3\mathrm{D}}$ is the 3D slope-safety factor; W is the weight of one column; A is the area of the slip surface; P is the vertical force acting on each column (the distributed force of upper load), here $P=0$; N is the normal force on each column; c is the cohesion; φ is the friction angle; θ is the dip (the normal angle of slip surface); θ_{Avr} is the apparent dip in the main inclination direction of the slip surface; θ_{Asp} is the dip direction of the grid column slip surface; θ_{AvrAsp} is the average dip direction of the slip surface and j and i are the numbers of row and column of the grid in the range of slope failure.

By analyzing the results, where the 3D safety factor is less than 1 (Table 1), the parameters of $c=20$ kN/m^2 and $\varphi=26°$ were chosen to represent the shear parameters of the sliding surface. These parameters will be used in the slope-stability analysis of the adjacent region.

Distribution of possible landslides

As the adjacent region has similar engineering geological conditions, we assume that the slope failure in this region has the same mechanism with the past landslide,

Table 1 Mechanical parameters and safety factor

Case (c, kN/m^3)	3D safety factor		
	Revised Hovland model	3D extension of Bishop model	3D extension of Janbu model
$c=20$, $\varphi=23°$	0.801	0.834	0.786
$c=21$, $\varphi=26°$	0.949	0.981	0.903
$c=19$, $\varphi=26°$	0.801	0.839	0.768
$c=23$, $\varphi=33°$	1.102	1.159	1.059
$c=19$, $\varphi=25°$	0.830	0.867	0.795
$c=22$, $\varphi=25°$	0.978	1.010	0.931
$c=21$, $\varphi=31°$	0.955	1.006	0.919
$c=24$, $\varphi=30°$	1.132	1.177	1.081

that is to say, the potential failure surface would develop along the interface between map units An-5 and An-7 under heavy rainfall. To detect the 3D critical slip surface of each slope unit, a search is performed by Monte Carlo simulation. The initial slip surface is assumed to be the lower part of an ellipsoid and changes according to multiple layer strengths and the conditions of the discontinuous surface. The five parameters that describe an ellipsoid are selected as random variables with uniform distribution: three-axial parameters "a, b, c," the central point "C" and the inclination angle "θ" of the ellipsoid (Fig. 7). The central point of the ellipsoid is first set as the central point of a slope unit, and then randomly chosen within a certain range. The critical slip surface is fulfilled by searching the parameter space of the 3D safety factor. If a randomly produced slip surface is lower than the interface of map units An-7 and An-5, it is limited by the interface itself.

Using the same engineering geological conditions of the past landslide, and the same triggering factor (rainstorm), the minimum 3D safety factor is calculated for each slope unit. Since a single value of safety factor is not sufficient enough for evaluating the slope stability of a slope unit, the ratio of the number of safety factor values less than 1.0 to the total times of calculation is calculated as the failure probability of the slope unit. If the failure probability is more than 80%, the slope unit is clarified as unstable (Fig. 8).

Two-dimensional numerical model of debris flow

Debris flows are rapidly flowing mixtures of water, clay and granular materials and often are mobilized from rainfall-induced landslide (Mainali and Rajaratnam 1994; Anderson 1995; Lan et al. 2004; Fiorillo and Wilson 2004; Fleming et al. 1989; Wen and Aydin 2005; Dai et al. 1999). The key requirements in the assessment of debris-flow risk consist of the predication of the flow trajectory over the complex topography, the potential run-out distance and the inundation area in order to define a safety zone. Numerical simulation models incorporating GIS are important prediction tools.

Governing equations

Based on the conservation of mass and the momentum of the flow, many authors have proposed mathematical models of the debris flow; some of them are 2D models(Takahashi et al. 1992; O'Brien et al. 1993; Chen and Lee 2000; Ghilardi et al. 2001; Denlinger and Iverson 2001). The rainfall-induced debris flow is often considered to move as a continuous fluid until stoppage rather than as a sliding solid (Takahashi et al. 1992; Hunt 1994; Hungr 1995; Laigle and Coussot 1997). The debris and water mixture is assumed to be a uniform continuous, incompressible, unsteady Newtonian fluid. The flow is governed by the continuity equation and the Navier–Stokes equations:

$$\nabla \mathbf{u} = \mathbf{0} \tag{4}$$

$$\rho \frac{\partial \mathbf{u}}{\partial t} + \rho \mathbf{u} \cdot \nabla \mathbf{u} = \rho \mathbf{g} - \nabla p + \mu \nabla^2 \mathbf{u} \tag{5}$$

where $\mathbf{u}=(u,v,w)$ is velocity; ρ is the mass density; p is the pressure; μ is dynamic viscosity; $\mathbf{g}=(0,0,g)$, g is the gravitational constant and t is time.

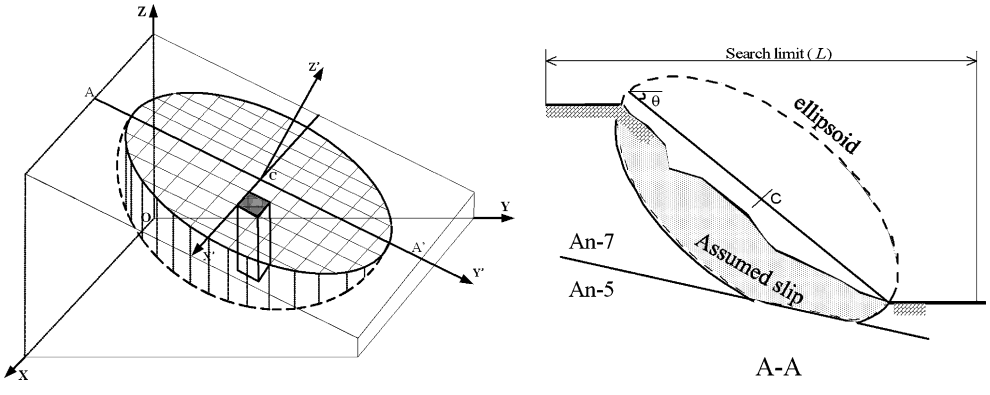

Fig. 7 Example of randomly produced ellipsoid used to simulate the 3D slide mass

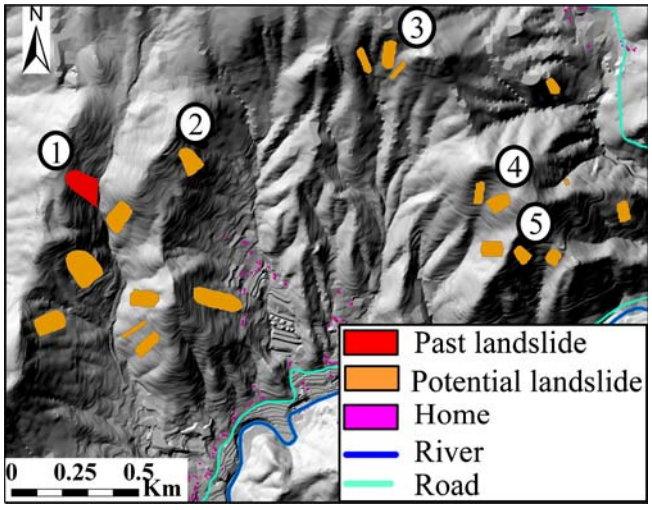

Fig. 8 Distribution of the past landslide and the 19 potential landslides

In order to simplify these equations, depth-averaged method is used to eliminate explicit dependence on the coordinate normal to the bed, z. Depth-averaged requires integrating each component equation from the base of the flow at $z = \eta_b$ to the surface of the flow at $z = \eta$ (Fig. 9). The pertinent mathematical manipulations are rather lengthy, and some details are omitted here. However, the details are similar to those in Vreugdenhil's (1994) derivation of the standard shallow-water equations and in Hutter et al.'s (1993) derivation of granular avalanche equations. The derivation makes frequent use of Leibniz theorem for interchanging the order of integrations and differentiations and of kinematic boundary conditions that specify that flow mass neither enters nor leaves at the free surface or base of the flow:

$$u\frac{\partial z}{\partial x} + v\frac{\partial z}{\partial y} - w = 0 \quad \text{at the base } z = \eta_b \tag{6}$$

$$\frac{\partial z}{\partial t} + u\frac{\partial z}{\partial x} + v\frac{\partial z}{\partial y} - w = 0 \quad \text{at the free } z = \eta \tag{7}$$

Herein, the depth-averaged velocities are defined as follows:

$$U = \frac{1}{h}\int_{\eta_b}^{\eta} u\,dz, \quad V = \frac{1}{h}\int_{\eta_b}^{\eta} v\,dz \tag{8}$$

Using these definitions and boundary conditions together with Eqs. 4 and 5, the following depth-averaged equations are developed to simulate the debris flow:

$$\frac{\partial h}{\partial t} + \frac{\partial M}{\partial x} + \frac{\partial N}{\partial y} = 0 \tag{9}$$

$$\frac{\partial M}{\partial t} + \alpha\frac{\partial (MU)}{\partial x} + \alpha\frac{\partial (MV)}{\partial y} = -\frac{\partial H}{\partial x}gh + \upsilon\beta\left(\frac{\partial^2 M}{\partial x^2} + \frac{\partial^2 M}{\partial y^2}\right) - gh\cos\theta_x \tan\xi \tag{10}$$

$$\frac{\partial N}{\partial t} + \alpha\frac{\partial (NU)}{\partial x} + \alpha\frac{\partial (NV)}{\partial y} = -\frac{\partial H}{\partial y}gh + \upsilon\beta\left(\frac{\partial^2 N}{\partial x^2} + \frac{\partial^2 N}{\partial y^2}\right) - gh\cos\theta_y \tan\xi \tag{11}$$

where $M = Uh$ and $N = Vh$ are the x- and y-components of the flow flux; U and V are the x- and y-components of the depth-averaged velocity; H is the height of the free surface; h is the flow depth; θ_x and θ_y are the angle of inclination at the bed along the x and y directions, respectively; α and β are the momentum correction factors; $\upsilon = \mu/\rho_d$ is kinematic viscosity, ρ_d is the equivalent density of the debris mixture, and $\rho_d = \rho_s v_s + \rho_w v_w$, ρ_s and ρ_w are the densities of solid grains and water, v_s and v_w are the volumetric concentrations of solids particles and water in the mixture; and $\tan\xi$ is the dynamic friction coefficient.

Numerical solution

Digital elevation models in GIS automatically extract topographic variables, such as basin geometry, stream networks, slope, aspect, flow direction, etc. from raster-elevation data. Three schemes for structuring the elevation data for DEMs are: TIN, grid networks and vector- or contour-based networks (Moore et al. 1991). The most widely used data structures are grid networks with rows and columns, where each cell contains a value representing information, such as elevation. The grid-

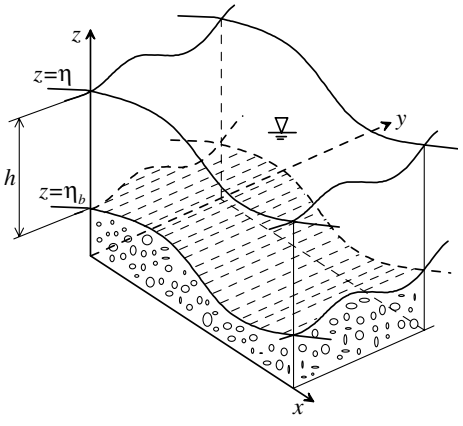

Fig. 9 Definition of coordinate system for 2D governing equations

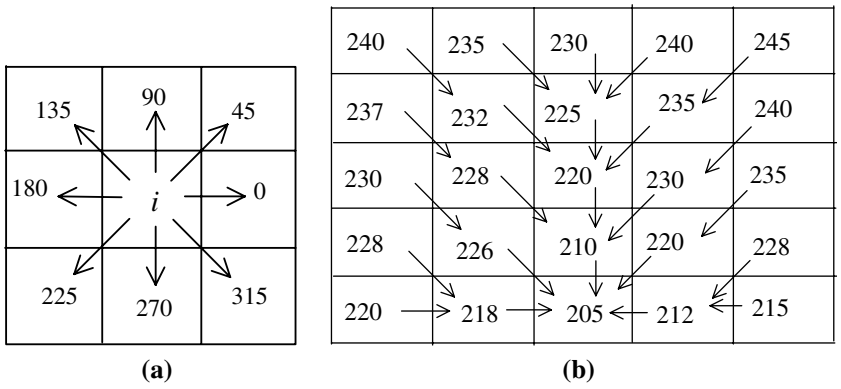

Fig. 10 Flow direction. **a** Possible flow direction in a cell. **b** Flow direction in a digital elevation model

based map of the studied area is immensely useful for numerical solution of the partial differential equations governing the propagation of debris flows. Finite-difference method on rectangular grids is widely used in numerical models of environmental flows. Therefore, in this paper, we used grid networks in GIS as the rectangular grids of finite-difference methods.

In a raster-based DEM analysis, each cell has eight possible flow directions (left, right, up, down, plus the four diagonals), as show in Fig. 10a. The flow direction of a cell is expressed in degrees: left = 0, up = 90 and right = 180, down = 270; and the diagonals: 45, 135, 225 and 315. Within a cell, overland flow is routed along one flow direction. The flow direction is the maximum downslope direction, which is determined from the raster-based DEM (Fig. 10b). The numerical solution is achieved using a finite-difference formulation based on the DEM grid. For a general 2D computation, as shown in Fig. 11, the finite-difference equations are: The continuity equation

$$\frac{h^{n+3}_{i+1/2,j+1/2}-h^{n+1}_{i+1/2,j+1/2}}{2\Delta t}+\frac{M^{n+2}_{i+1,j+1/2}-M^{n+2}_{i,j+1/2}}{\Delta x}+\frac{N^{n+2}_{i+1/2,j+1}-N^{n+2}_{i+1/2,j}}{\Delta y}=0 \tag{12}$$

And the momentum equation of x-component

$$\begin{aligned}&\frac{M^{n+2}_{i,j+1/2}-M^{n}_{i,j+1/2}}{2\Delta t}+\frac{\alpha}{\Delta x}\left[\left(\frac{M^{n}_{i+1,j+1/2}+M^{n}_{i,j+1/2}}{2h^{n+1}_{i+1/2,j+1/2}}\right)^2-\left(\frac{M^{n}_{i,j+1/2}+M^{n}_{i-1,j+1/2}}{2h^{n+1}_{i-1/2,j-1/2}}\right)^2\right]\\&+\frac{\alpha}{\Delta y}\left[\frac{\left(M^{n}_{i,j+1/2}+M^{n}_{i,j+3/2}\right)\left(N^{n}_{i+1/2,j+1}+N^{n}_{i-1/2,j+1}\right)}{h^{n+1}_{i-1/2,j+1/2}+h^{n+1}_{i+1/2,j+1/2}+h^{n+1}_{i+1/2,j+3/2}+h^{n+1}_{i-1/2,j+3/2}}-\frac{\left(M^{n}_{i,j+1/2}+M^{n}_{i,j-1/2}\right)\left(N^{n}_{i+1/2,j}+N^{n}_{i-1/2,j}\right)}{h^{n+1}_{i-1/2,j-1/2}+h^{n+1}_{i+1/2,j-1/2}+h^{n+1}_{i+1/2,j+1/2}+h^{n+1}_{i-1/2,j+1/2}}\right]\\&=-g\frac{\left(h^{n+1}_{i+1/2,j+1/2}+h^{n+1}_{i-1/2,j+1/2}\right)\left(H^{n+1}_{i-1/2,j+1/2}-H^{n+1}_{i-1/2,j+1/2}\right)}{2\Delta x}+\\&\frac{lon\beta}{2}\left[\frac{M^{n+2}_{i-1/2,j+1/2}+M^{n+2}_{i,j+3/2}-2M^{n+2}_{i,j+1/2}}{(\Delta x)^2}+\frac{M^{n+2}_{i,j-1/2}+M^{n+2}_{i,j+3/2}-2M^{n+2}_{i,j+1/2}}{(\Delta y)^2}\right]\\&-g\frac{h^{n+1}_{i+1/2,j+1/2}+h^{n+1}_{i-1/2,j+1/2}}{2}\cos\theta_x\tan\varphi\end{aligned} \tag{13}$$

An analogous finite-difference expression represents the momentum equation of y-component in Eq. 11.

Simulation of the real debris flow

The above approach is used to simulate the real debris flow that occurred at Minamata–Hougawachi. In this simulation, the depth of the landslide mass is assumed as the initial thickness of flow and the rheological parameters are set constant throughout the duration of the

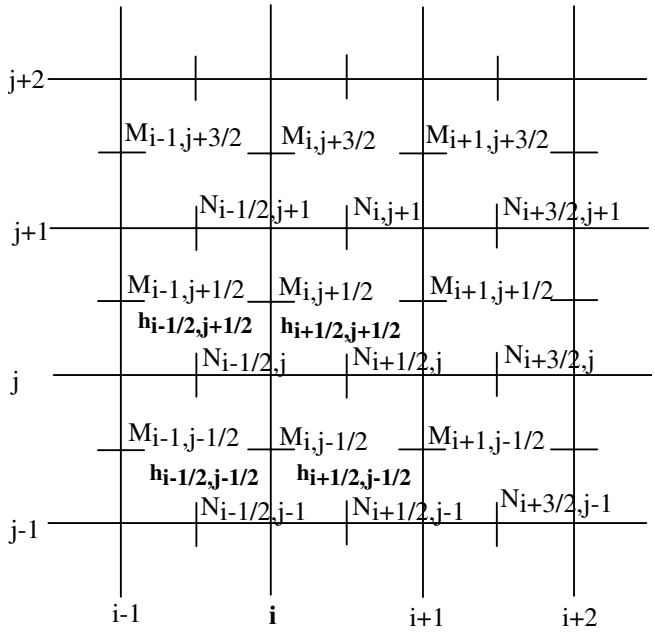

Fig. 11 Grids for 2D debris-flow computation

flow event (Table 2). As a result, the simulated debris flow takes 230 s to travel about 1,500 m along the stream with an average flow velocity of about 6.5 m/s. The development of the simulated debris flow is illustrated in Fig. 12 as a function of time. Figure 13a shows the simulated inundated area. Compared with the actual propagation of the debris flow (Fig. 13b), the simulation result shows positive identification. This means that the selected approach can be properly used to simulate debris flow triggered by rainstorm in the study area.

Influence of the volume of landslide mass on debris flow

In debris flow hazard assessment, the debris flow volume is one of the most important parameters, because it controls the characteristics of a debris flow, such as the peak discharge, the mean flow velocity, the impact force and the inundated area (Rickenmann 1999). For the debris flow triggered by landslide and rainfall, the debris-flow volume consists of the landslide mass (debris mixtures) volume and water volume. As a rough approximation, the maximum volume of landslide mass of the Minamata–Hougawachi landslide is 1,000,000 m^3

Table 2 Material properties and rheological parameters for simulation

ρ (kg/m^3)	α	β	μ (Pa s)	g (m/s^2)	tan ξ
2,200	1.25	1.0	0.11	9.8	0.6

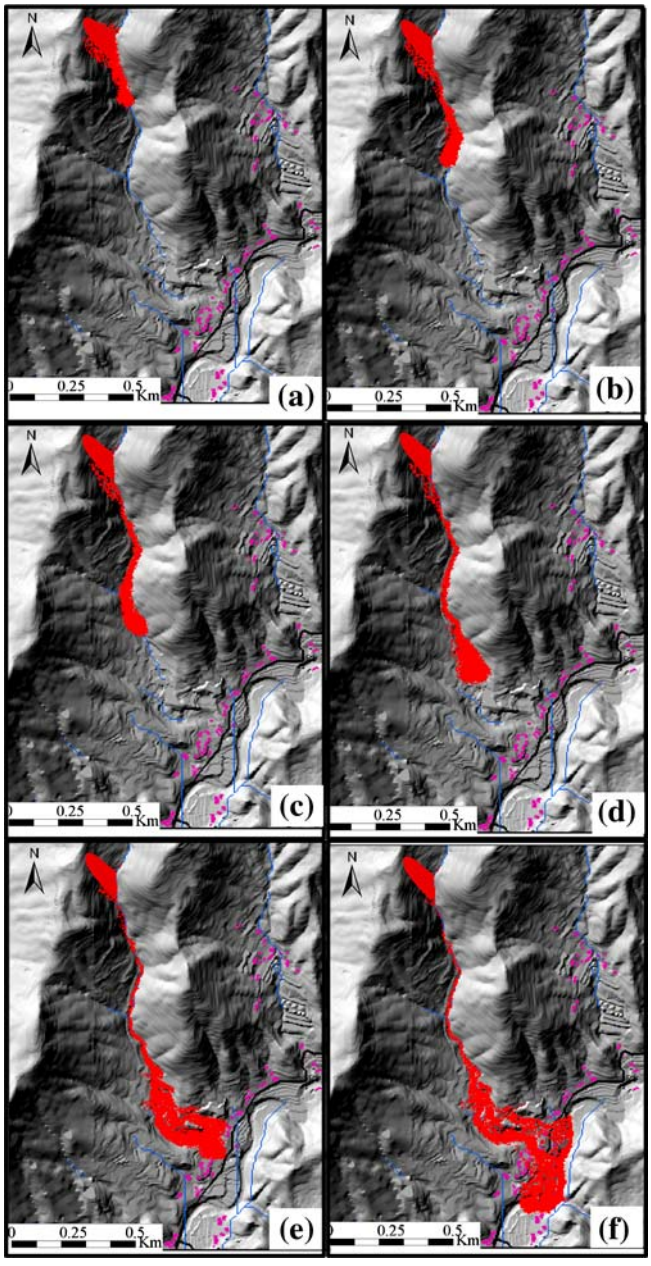

Fig. 12 Simulation of debris flow propagation in region of the actual Minamata–Hougawachi region debris flow (**a** 30 s, **b** 60 s, **c** 90 s, **d** 120 s, **e** 180 s and **f** 220 s)

(Taniguchi 2003). According to the landslide-size classification proposed by Fell (1994), it is considered as a very large landslide. The volume of landslide mass can be estimated using the sediment concentration of the flow. Coussot and Meunier (1996) suggest sediment concentrations of 0.45–0.8 (volume of sediment/volume of water and sediment), which yields the water volume of 200,000–550,000 m^3. The influence of the volume of landslide mass on the inundated area was evaluated by

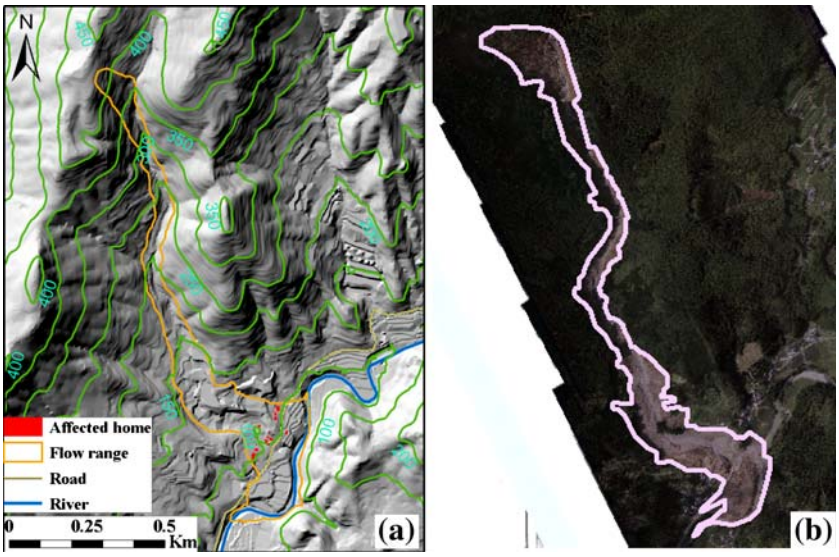

Fig. 13 Inundated area of the debris flow in Minamata–Hougawachi (**a** by the simulation and **b** by aerial photograph)

performing several numerical simulations. The results show a strong relation between the debris volume of the source area and the inundated area (Fig. 14).

Debris-flow hazard map

Assuming the pattern of landslide disasters in the Minamata–Hougawachi region is the same as the landslide of July 20, 2003, namely, the slope-sliding mass combining with the mountain torrent forms a debris flow passing along the stream valley, five stream valleys that are the most likely to be affected by these processes are recognized. For each stream valley, there are several potential landslide areas upriver. Because they are unlikely to fail at the same time, only one potential landslide was selected to simulate the inundated area for each stream valley (cases 1–5, numbered in Fig. 8). Case 1 (Fig. 8) is the real debris flow and has been simulated in the above section. Using the parameters calibrated by the historic landslide, four debris flows from the unstable slope units are simulated (cases 2–5). For these simulations, the flow times and distances are listed in Table 3, and the propagation processes of the debris flows is illustrated in Fig. 15. Finally, the debris-flow hazard zones are mapped in Fig. 16, in which the inundated areas of the debris flows, the potentially affected homes and road sections are shown.

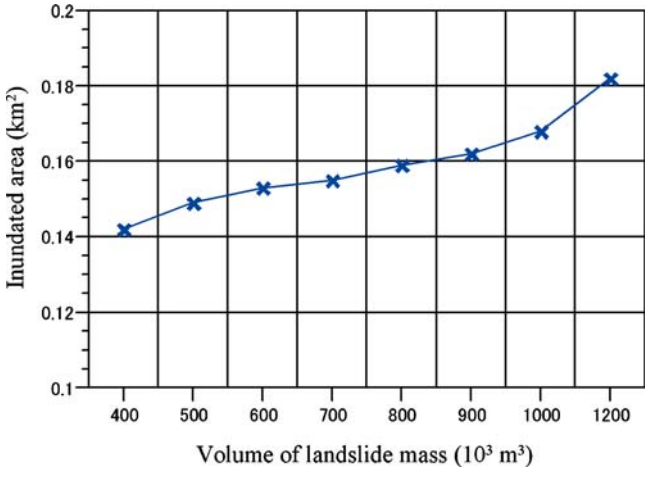

Fig. 14 Influence of the volume of landslide mass on inundated area

Conclusions

The field survey following July 20, 2003, disaster in the Minamata–Hougawachi region of Kumamoto Prefecture provides an insight into typical landslide mechanisms of the study area. Where map unit An-5 is overlain by map unit An-7 appears prone to landslide, particularly during high-intensity rainfall events during which the rainwater can seep within the seriously weathered An-7. When the pore-water pressure develops at the contact of the impermeable An-5, a landslide may potentially occur along the interface between An-7 and An-5.

Based on the study of the landslide of July 20, 2003, the parameters for 3D slope-stability analysis are back calculated. To locate the potential landslides, the study

Table 3 Flow time and distance for cases 2–5

	Case 2	Case 3	Case 4	Case 5
Time (s)	160	180	100	50
Distance (m)	1,100	1,300	700	400
Average velocity (m/s)	6.9	7.2	7.0	8.0

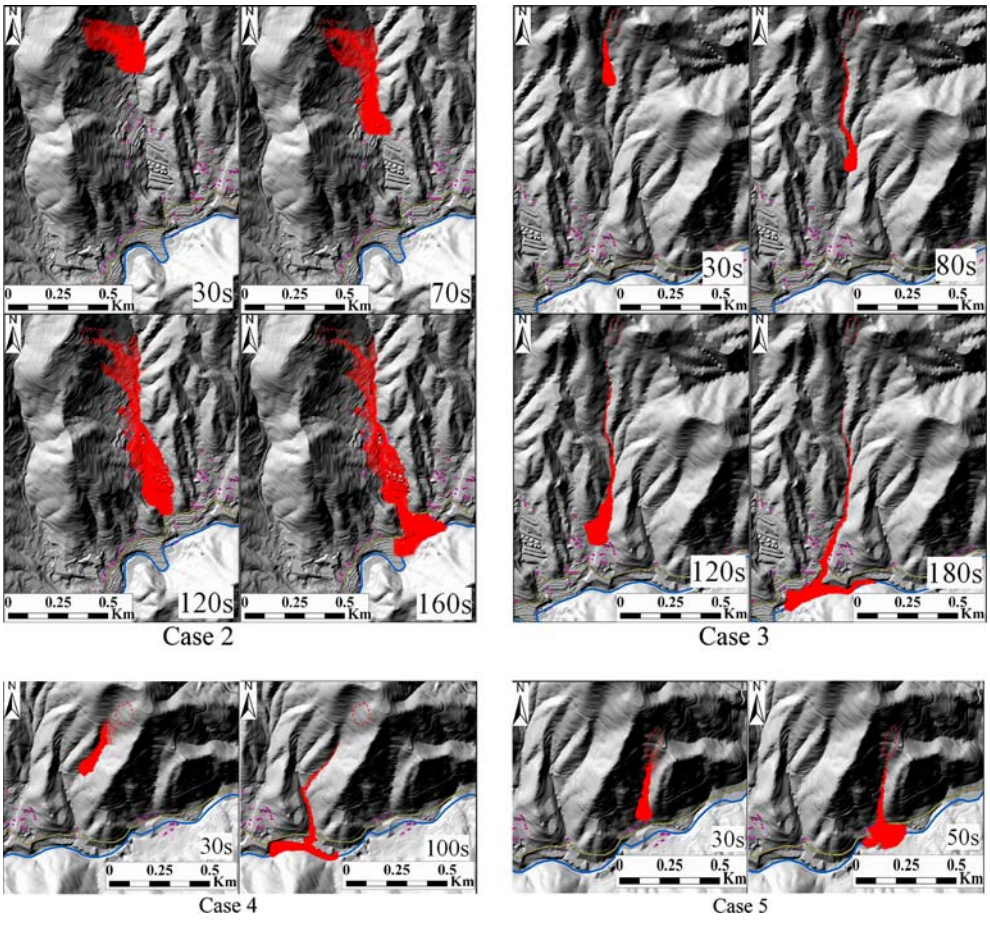

Fig. 15 Inundated areas of simulated potential debris flows (cases 2–5)

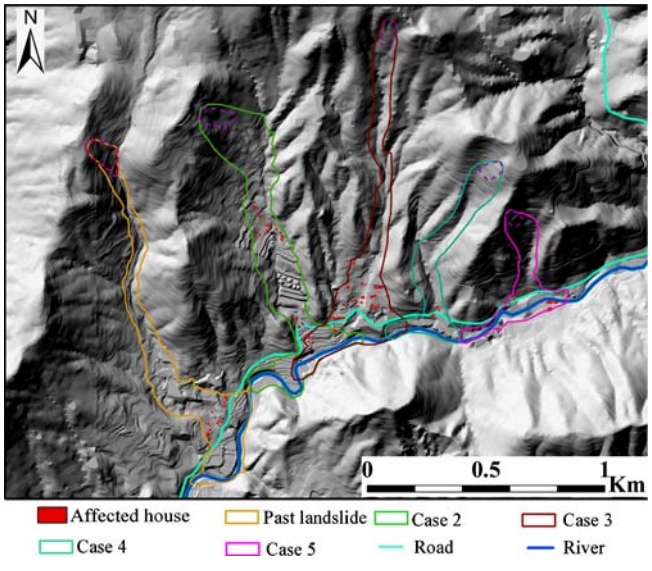

Fig. 16 Landslide-hazard map with distribution of homes, river and road

area is divided into slope units using the hydrologic analysis tool in ArcGIS, and using the GIS-based of the 3D limit-equilibrium model for slope-stability analysis and a Monte Carlo simulation, the location of potential landslides are obtained.

Most of the debris flows originally occur in the form of rainfall-induced landslides before they move into the valley channel. In order to define a debris-flow safety zone, the key requirements consist of the predication of the flow trajectory over the complex topography, the potential debris-flow run-out distance and the inundation area. In this paper, we developed a depth-averaged 2D numerical model incorporating a GIS. As raster-grid networks of DEM in GIS can be used as the finite-difference mesh, the continuity and momentum equations are solved numerically using the finite-difference method. The simulation method is used to model the propagation of the debris flow designed to emulate the historic debris flow. The results accurately model the historic debris flow. We also use this simulation procedure to model potential landslides that might form debris flows in other stream valleys in the Minamata–Hougawachi region. Using the parameters calibrated by the past landslide,

four debris flows from unstable slope units are simulated (cases 2–5). According to the results of debris-flow simulation, the potential inundation area is modeled, mapping the potentially affected homes, streams and roads. Since the actual inundated areas are controlled by the volume of the landslide mass, the rainfall amount and the regional terrain following any actual landslide, there can be some uncertainties when forecasting the affected areas in this study. The simulation method developed here allows many model runs to be performed and scenarios based on many different events occurring in many locatons could be developed.

References

Aleotti P, Chowdhury R (1999) Landslide hazard assessment: summary review and new perspectives. Bull Eng Geol Environ 58:21–44

Anbalagan R (1992) Landslide hazard evaluation and zonation mapping in mountainous terrain. Eng Geol 32:269–277

Anderson SA (1995) Analysis of rainfall-induced debris flows. J Hydraulic Eng 121:544–552

Bergin DO, Kimberley MO, Marden M (1995) Protective value of regenerating tea tree stands on erosion-prone hill country, East Coast, North Island, New Zealand. N Z J For Sci 25:3–19

Carrara A, Guzzetti F (1999) Use of GIS technology in the prediction and monitoring of landslide hazard. Nat Hazards 20:117–135

Carrara A, Cardinali M, Detti R, Guzzetti F, Pasqui V, Reichenbach P (1991) GIS techniques and statistical models in evaluating landslide hazard. Earth Surf Process Landforms 16:427–445

Chen H, Lee CF (2000) Numerical simulation of debris flows. Can Geotech J 37:146–160

Coussot P, Meunier M (1996) Recognition, classification and mechanical description of debris flows. Earth-Sci Rev 40:209–227

Dai F, Lee CF, Wang S (1999) Analysis of rainstorm-induced slide-debris flows on natural terrain of Lantau Island, Hong Kong. Eng Geol 51:279–290

David, RM (2002) Arc hydro: GIS for water resources. ESRI, Redlands

Denlinger RP, Iverson RM (2001) Flow of variably fluidized granular masses across three-dimensional terrain. J Geophys Res 106:553–566

Dymond JR, Derose RC, Harmsworth GR (1995) Automated mapping of land components from digital elevation data. Earth Surface Processes Landforms 20:131–137

Fell R (1994) Landslide risk assessment and acceptable risk. Can Geotech J 31:261–272

Fiorillo F, Wilson RC (2004) Rainfall induced debris flows in pyroclastic deposits, Campania (southern Italy). Eng Geol 75:263–289

Fleming RW, Ellen SD, Algus MA (1989) Transformation of dilative and contractive landslide debris into debris flow—an example from Marin Country, California. Eng Geol 27:201–223

Ghilardi P, Natale L, Savi F (2001) Modeling debris flow propagation and deposition. Phys Chem Earth 26:651–656

Guariguata MR (1990) Landslide disturbance and forest regeneration in the Upper Luquillo Mountains of Puerto Rico. J Ecol 78:814–832

Guzzetti F, Carrara A, Cardinal M, Reichenbach P (1999) Landslide evaluation: a review of current techniques and their application in a multi-scale study, Central Italy. Geomorphology 31: 181–216

Hansen A (1984) Landslide hazard analysis. In: Brunsden D, Prior DB (eds) Slope instability. Wiley, New York, pp 523–602

Hungr O (1995) A model for the runout analysis of rapid flow slides, debris flows and avalanches. Can Geotech J 32(4):610–623

Hunt B (1994) Newtonian fluid mechanics treatment of debris flows and avalanches. J Hydraulic Eng 120:1350–1363

Hutchinson JN (1995) Landslide hazard assessment. Keynote paper. In: Bell DH (ed) Landslides, Proceeding of 6th international symposium on landslides, Christchurch, New Zealand, vol 1. Balkema, Rotterdam, pp 1805–1841

Hutter K, Siegel M, Savage SB, Nohguchi Y (1993) Two-dimensional spreading of a granular avalanche down an inclined plane, Part I theory. Acta Mech 100:37–68

Iida T (1999) A stochastic hydro-geomorphological model for shallow landsliding due to rainstorm. Catena 34: 293–313

Iwao Y (2003) Slope hazard induced by heavy rain in 2003, Minamata city, Kumamoto (in Japanese). J Jpn Landslide Soc 40:239–240

Laigle D, Coussot P (1997) Numerical modeling of mudflows. J Hydraulic Eng 123:617–623

Lan HX, Zhou CH, Wang LJ, Zhang HY, Li RH (2004) Landslide hazard spatial analysis and prediction using GIS in the Xiaojiang watershed, Yunnan, China. Eng Geol 76:109–128

Mainali A, Rajaratnam N (1994) Hydraulics of debris flows. J Hydraulic Eng 120:104–123

Moore ID, Grayson RB, Ladson AR (1991) Digital terrain modeling: a review of hydrological, geomorphological and biological applications. Hydrol Processes 5:3–30

Nakazawa T, Saito M, Taguchi Y (2003) Geologic and hydrologic background of slope failure and debris-flow disaster in Atsumari River Basin, Minamata City, Kumamoto Prefecture on July 20, 2003 (in Japanese). Bull Geol Surv Jpn 55:113–127

O'Brien JP, Julien PJ, Fullerton WT (1993) Two-dimensional water flood and mudflow simulation. J Hydraulic Eng 119:244–261

Rickenmann D (1999) Empirical relationships for debris flows. Nat Hazards 19:47–77

Takahashi T, Nakagawa H, Harda T, Yamashiki Y (1992) Routing debris flows with particle segregation. J Hydraulic Eng 118:1490–1507

Taniguchi Y (2003) Debris disaster caused by local heavy rain in Kyushu area on July 20th, 2003 (prompt report), Minamata debris disaster (in Japanese). J Jpn Soc Erosion Control Eng 56:31–35

Vreugdenhil CB (1994) Numerical methods for shallow-water flow. Kluwer Academic Publishers, Norwell

Walker LR, Zarin DJ, Fetcher N, Myster RW, Johnson AH (1996) Ecosystem development and plant succession on landslides in the Caribbean. Biotropica 28:566–576

Wen BP, Aydin A (2005) Mechanism of a rainfall-induced slide-debris flow: constraints from microstructure of its slip zone. Eng Geol 78:69–88

Xie M, Esaki T (2005) GIS-based 3D slope evaluation and landslide hazard assessment. Kyushu University, Fukuoka, Japan

Xie M, Esaki T, Zhou G, Mitani Y (2003) Geographic information systems-based three-dimensional critical slope stability analysis and landslide hazard assessment. J Geotech Geoenviron Eng, ASCE 129:1109–1118

Zhou G, Esaki T, Mitani Y, Xie M, Mori J (2003) Spatial probabilistic modeling of slope failure using an integrated GIS Monte Carlo simulation approach. Eng Geol 68:373–386